Noncollinear spin structure with weak ferromagnetism in NbMnP

Masaaki Matsuda, Depei Zhang, Yoshiki Kuwata, Qiang Zhang, Takahiro Sakurai, Hitoshi Ohta, Hitoshi Sugawara, Keiki Takeda, Junichi Hayashi, and Hisashi Kotegawa

Phys. Rev. B **104**, 174413 — Published 9 November 2021

DOI: 10.1103/PhysRevB.104.174413

Noncollinear spin structure with weak ferromagnetism in NbMnP

Masaaki Matsuda,[1] Depei Zhang,[1] Yoshiki Kuwata,[2] Qiang Zhang,[1] Takahiro Sakurai,[3] Hitoshi Ohta,[2,4] Hitoshi Sugawara,[2] Keiki Takeda,[5] Junichi Hayashi,[5] and Hisashi Kotegawa[2]

[1]*Neutron Scattering Division, Oak Ridge National Laboratory, Oak Ridge, Tennessee 37831, USA*
[2]*Department of Physics, Kobe University, Kobe, Hyogo 658-8530, Japan*
[3]*Research Facility Center for Science and Technology, Kobe University, Kobe, Hyogo 657-8501, Japan*
[4]*Molecular Photoscience Research Center, Kobe University, Kobe, Hyogo, 657-8501, Japan*
[5]*Muroran Institute of Technology, Muroran, Hokkaido 050-8585, Japan*

(Dated: October 19, 2021)

NbMnP is a metallic material, which consists of the zigzag chains of Mn moments along the b axis. The magnetic susceptibility as well as the resistivity shows an anomaly at 233 K, which indicates an antiferromagnetic phase transition. Our neutron powder diffraction experiment reveals that the magnetic structure is a Q=0 structure and noncollinear with an easy plane anisotropy perpendicular to the b axis and the a and c axis magnetic components align antiferromagnetically and ferromagnetically along the zigzag chain direction, respectively. The ordered moment is 1.2$\mu_{\rm B}$, which is reduced probably due to the itineracy of the Mn moments. A localized picture model suggests that the Q=0 magnetic structure is formed by the frustration among several exchange couplings. A weak ferromagnetic component is also present in the antiferromagnetic phase, which is considered to be caused by a Dzyaloshinskii-Moriya interaction.

I. INTRODUCTION

The Dzyaloshinskii-Moriya (DM) interaction, which is an antisymmetric exchange coupling originating from the combination of a lack of inversion symmetry and spin-orbit coupling [1, 2], was first argued to explain weak ferromagnetism in some antiferromagnetic materials. Absence or presence of the DM interaction is primarily evaluated depending on whether the crystal symmetry has inversion center or not, respectively. However, even when the crystal structure has an inversion symmetry, in the sublattice constructed by an equivalent magnetic interaction, such as second neighbor or third neighbor interaction, the center of the bonds can lack inversion symmetry, which leads to the DM character of the interaction [3]. The DM interaction causes not only canted weak ferromagnetism but also gives rise to other non-collinear magnetic structures, such as helical state. Interestingly, the DM interaction acts as a driving force for novel phenomena.

One example is the magnetic skyrmion lattice, which exhibits various interesting properties, including novel Hall effect and multiferroic behavior, and has attracted much attention because of its possibility for industrial application in spintronic devices [4]. MnSi is a prototypical material, exhibiting the skyrmion lattice phase just below the antiferromagnetic transition temperature in finite magnetic fields [5]. A helical structure is the magnetic ground state at ambient field. A DM interaction is ascribed to the formation of the helical structure [6] as well as the skyrmion lattice [5].

NbMnP has the TiNiSi-type orthorhombic structure (space group $Pnma$) [7] with inversion symmetry, in which Mn atoms form zigzag chains along the b axis, as shown in Fig. 1. From this structure, one would expect frustrated magnetic interactions between the nearest-neighbor and second-neighbor couplings in the zigzag chain, which might give rise to interesting magnetic and transport properties. The DM interactions can also be present for the second, third, and fourth-neighbor interactions. However, the physical properties of this material have not been studied so far. Therefore, it is important to characterize the bulk properties and determine the magnetic structure in NbMnP to discuss the mechanism and effect of the frustrated interactions.

Very small pieces of NbMnP single crystals were grown and the magnetic properties were characterized. The magnetic susceptibility shows a small increase at 233 K [Fig. 2(a)], indicating an antiferromagnetic magnetic ordering with a weak ferromagnetic component. Neutron powder diffraction study was performed to determine the magnetic structure using a bunch of the small crystals. We observed commensurate magnetic peaks with $\boldsymbol{Q}_{\mathbf{m}}$=(0, 0, 0). The magnetic structure was found to be a noncollinear antiferromagnetic structure with magnetic moments confined in the ac plane, in which arrangements of magnetic components along the a axis and c axis are antiferromagnetic and ferromagnetic along the zigzag chain direction, respectively, with the ordered magnetic moment of 1.2$\mu_{\rm B}$ at 9 K. The reduced moment indicates itineracy of the Mn moments. Although we anticipated a competition between the nearest-neighbor and second-neighbor interactions in the zigzag chain, the magnetic structure suggests competing intrachain and interchain couplings. DM interactions may also be at work to realize the noncollinear magnetic structure in the ac plane as well as the weak ferromagnetism. NbMnP is an interesting material with the frustrated and DM interactions for itinerant Mn moments.

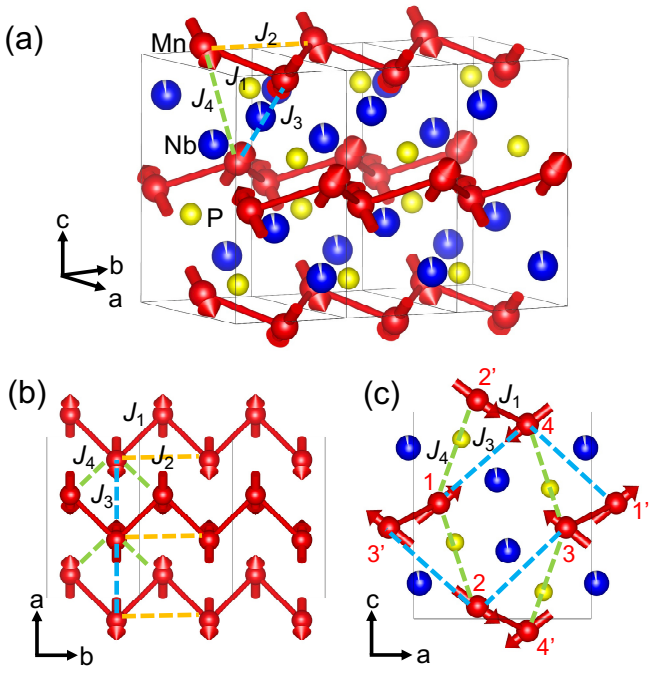

FIG. 1. (a) Crystal and magnetic structures of NbMnP. The structural parameters are shown in Table I. (b) and (c) are the structures projected along the c and b directions, respectively. The bold lines are bonds between nearest-neighbor Mn atoms, which form zigzag chains along the b axis. The magnetic interactions (J_1, J_2, J_3, and J_4) are indicated. Nonmagnetic atoms are removed in (b) to display the Mn-Mn interactions clearly. The numbers in (c) represent four inequivalent Mn sites in a unit cell. The numbers with the prime symbol represent Mn sites in the neighboring unit cell.

II. EXPERIMENTAL DETAILS

Single crystals of NbMnP were grown using the self-flux method similar to that in Ref.[8]. Starting materials of Nb powder, Mn powder and P flakes with the molar ratio of 2.5 : 85.9 : 12.85 were put into Al_2O_3 crucible and sealed into an evacuated quartz ampoule. The ampoule was gradually heated up to 1200 °C and held at this temperature for 6 h. Then it was slowly cooled down to 900 °C with a rate of −3.3 °C/h. Excess substances were decomposed using diluted nitric acid solution or mixed solution of acetic acid and hydrogen peroxide. Some single crystals grown using this method have short needle-like shape with the length less than 0.5 mm. However, most of the small single crystals, used for the neutron powder diffraction measurements, are broken into random-shaped pieces in the process of the excess substance removal. The X-ray diffraction and resistivity measurements were performed using a single crystal. However, since the crystals were too small to measure magnetic susceptibility and also observe magnetic Bragg peaks with neutron diffraction measurement, we used a bunch of the small single crystals without crushing for the magnetic susceptibility and neutron powder diffraction measurements.

Magnetic susceptibility was measured in the temperature range between 2 and 300 K and the field range between 0.1 and 5 T using MPMS. Resistivity was measured using the 4 terminal method in the temperature range between 1.6 and 295 K at ambient field. X-ray diffraction measurement was performed at 200 and 293 K using Rigaku Saturn724 diffractometer with a multilayer mirror monochromated Mo-Kα radiation at room temperature. The program suite SHELX was used for structure solution and least-squares refinement [9]. Platon was also used to check for missing symmetry elements in structures [10].

Neutron powder diffraction was measured at 9, 150, and 250 K using 2.2-gram sample on the time-of-flight powder diffractometer POWGEN [11] with a neutron wavelength band of 0.970-2.033 Å. A closed-cycle refrigerator was used to cool down the sample. For magnetic structure analysis, the representational analysis was performed using the BasIreps package [12]. Rietveld refinements were performed for the neutron powder diffraction data using the FullProf package [13].

III. EXPERIMENTAL RESULTS

A. Bulk Properties

We first performed the X-ray diffraction measurements using a single crystal. The crystal structure of our NbMnP sample was confirmed to be *Pnma* both at 293 K in the paramagnetic phase and 200 K in the antiferromagnetic phase. The determined structural parameters, shown in Table I, are consistent with the previous results reported in Ref. [7]. It is interesting that the lattice constants are not contracted homogeneously with cooling down. Comparing the lattice constants at 200 and 293 K, b is contracted by 0.19% but c is expanded by 0.15% at 200 K, whereas a is just slightly expanded by 0.03%. These lattice changes along the b and c axes are consistent with those observed with the powder neutron diffraction measurements at 9 and 250 K, as shown in APPENDIX. This indicates a magnetoelastic coupling in the magnetically ordered state. These structural parameters will be used to discuss the magnetic interactions in NbMnP in Sec. IV.

Figure 2(a) shows the magnetic susceptibility in NbMnP. Since a bunch of non-aligned single crystals were used, the result is equivalent to that from a powder sample and no information of the anisotropy can be obtained. The susceptibility abruptly increases below ∼233 K. As shown in the inset of Fig. 2(b), the increase of the susceptibility is suppressed at higher magnetic field and above 2 T the susceptibility just shows a cusp at 233 K. These indicate that the magnetic structure should be mainly antiferromagnetic with T_N ∼233 K, and it is accompanied by a small ferromagnetic component. This assumption is consistent with a slight decrease of the magnetic

TABLE I. Structural parameters of NbMnP determined by the X-ray structural analysis at T=293 K and 200 K.

$T = 293$ K						
Atom	position	x	y	z	$Occ.$	U(Å^2)
Nb	4c	0.03102(5)	0.25000	0.67215(5)	0.968	0.00582(15)
Mn	4c	0.14147(9)	0.25000	0.05925(8)	1	0.0063(2)
P	4c	0.26798(15)	0.25000	0.36994(13)	1	0.0061(2)

orthorhombic ($Pnma$): a=6.1823(2) Å, b=3.5573(2) Å, c=7.2187(3) Å, R=1.90%

$T = 200$ K						
Atom	position	x	y	z	$Occ.$	U(Å^2)
Nb	4c	0.03123(6)	0.25000	0.67187(5)	0.969	0.00486(18)
Mn	4c	0.14152(9)	0.25000	0.05945(8)	1	0.0053(2)
P	4c	0.26790(15)	0.25000	0.36949(14)	1	0.0052(3)

orthorhombic ($Pnma$): a=6.1841(3) Å, b=3.5504(2) Å, c=7.2295(4) Å, R=2.25%

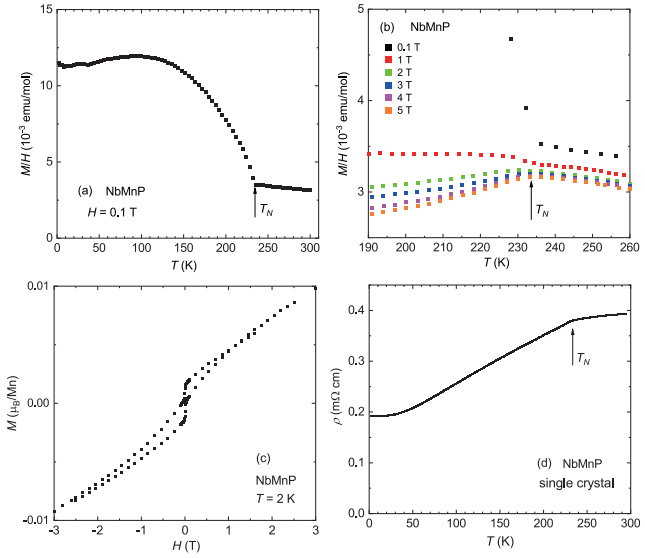

FIG. 2. (a) Temperature dependence of magnetic susceptibility M/H measured using a bunch of non-aligned single crystals at 0.1 T, showing a kink at $T_{\rm N}$ = 233 K. (b) M/H versus temperature as a function of magnetic field near $T_{\rm N}$. (c) Magnetization curves measured at 2 K, showing a small ferromagnetic component. (d) Temperature dependence of electrical resistivity for a single crystal, which also shows a clear anomaly at $T_{\rm N}$.

susceptibility below ∼100 K, which indicates that the susceptibility decreases due to the antiferromagnetic order with the weak ferromagnetic component saturated at low temperatures. The magnitude of the ferromagnetic component is very small ($\sim 0.0015\mu_{\rm B}$/f.u.), as confirmed by the residual magnetization in the magnetization curve at 2 K shown in Fig. 2(c). A small upturn of the magnetic susceptibility below ∼10 K probably originates from paramagnetic impurities.

The electrical resistivity is shown in Fig. 2(d). The resistivity decreases abruptly below $T_{\rm N}$. Compared with a material with the same TiNiSi-type structure and other Mn-based materials, the absolute value of the resistivity at room temperature in NbMnP is similar to those in NbCrP [14] and Mn_3Sn[15] but a few times larger than those in MnP [16], Mn_3P [17], and MnSi [18].

B. Magnetic Structure

In order to determine the magnetic structure of NbMnP, neutron powder diffraction measurements were performed above and below $T_{\rm N}$(=233 K). The refined structural parameters are summarized in APPENDIX. As shown in Fig. 3, the neutron diffraction patterns of NbMnP were collected at 9, 150, and 250 K. We found increase of (100) (Q ∼1.02 Å^{-1}), (110) (Q ∼2.05 Å^{-1}), (012) (Q ∼2.48 Å^{-1}), and (300) (Q ∼3.05 Å^{-1}) Bragg peak intensities at low temperatures. This indicates that these are magnetic signals with $\boldsymbol{Q}_{\mathbf{m}}$=(0, 0, 0), meaning that the magnetic unit cell is the same as the primitive unit cell. The magnetic intensity at 150 K is slightly reduced compared to that at 9 K, but the relative intensities do not change with temperature. This suggests that the magnetic structure is not temperature dependent but only the ordered magnetic moment is reduced with increasing temperature.

Since the crystal symmetry below $T_{\rm N}$ was experimentally determined to be $Pnma$, as shown in Table I, representational analysis was performed for $Pnma$ and $\boldsymbol{Q}_{\mathbf{m}}$=(0, 0, 0). There are four Mn sites in a unit cell, as indicated in Fig. 1(c). The possible magnetic structures are listed in Table II. We found that two irreducible representations Γ_6 + Γ_7, where Γ_6 with w=0 and Γ_7 with u=0 represent the a and c axis moment components, respectively, are dominantly needed to reproduce the magnetic intensities. Γ_7 with u=0 is primarily needed to reproduce the large (100) intensity. Γ_6 with w=0 contributes to increase the (110) intensity. Although finite w in Γ_6 and u in Γ_7 can be present in principle, we just used u in Γ_6 and w in Γ_7 and assumed that w in Γ_6 and u in Γ_7 are zero in order to reduce the number of

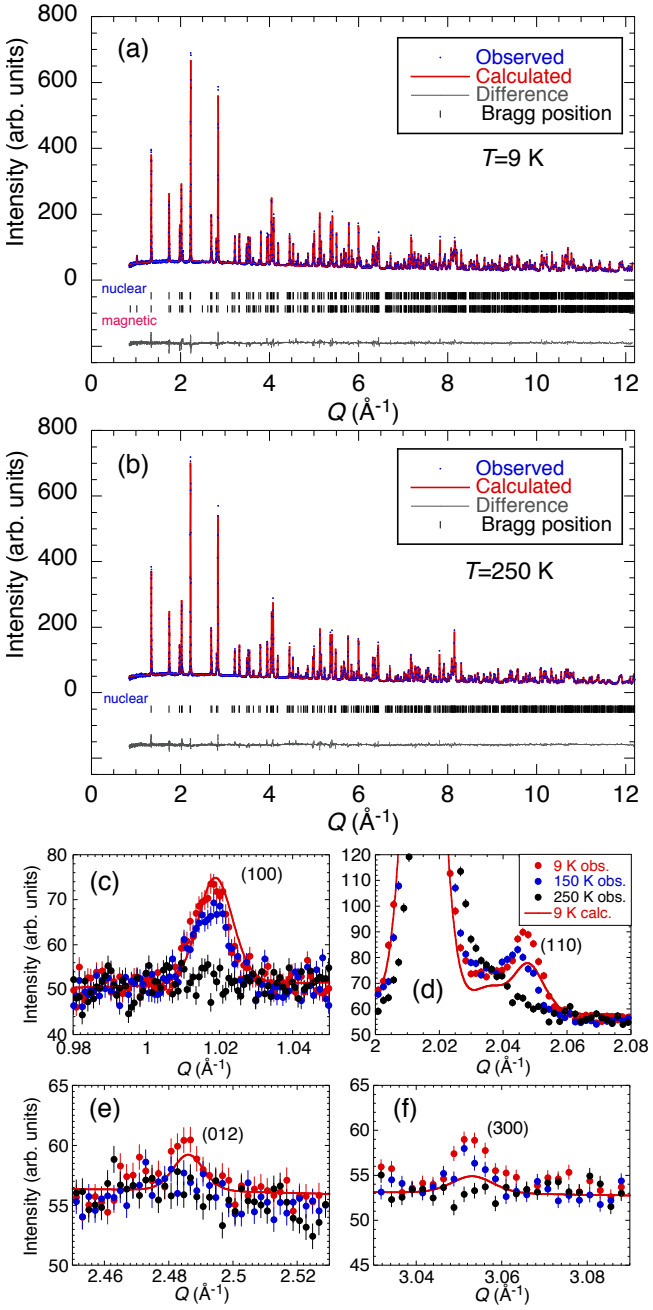

FIG. 3. Neutron powder diffraction of NbMnP at 9 K (a) and 250 K (b). Observed (blue dots), calculated (red line), and difference (gray line) patterns from Rietveld analyses. The vertical bars are Bragg peak positions expected from the nuclear and magnetic structures. The nuclear Bragg R factor at 250 K is 6.24%. The magnetic R factor at 9 K is 13.3% with the nuclear Bragg R factor of 5.30%. Temperature dependences of three magnetic Bragg peaks, (100) (c), (110) (d), (012) (e), and (300) (f). The solid lines in (c), (d), (e), and (f) represent calculated intensities with the moments along the a and c axes being $0.83(7)\mu_B$ and $0.88(5)\mu_B$, respectively.

fitting parameters. The magnetic stricture with the two irreducible representations may be related with the magnetoelastic coupling, as described in Sec. IIIA, which is considered to occur to relieve the magnetic frustration. For the Rietveld fitting, there is an ambiguity of choosing Mn valence state for the magnetic form factor. We evaluated all possible valence states for Mn and found that Mn^{3+} and Mn^{4+} yield almost equally good R factors, which are better than those for other valence states. Since the accurate valence state is not known in NbMnP, we will show the results obtained with Mn^{3+}.

Because of the magnetic propagation vector being (0, 0, 0), most of the magnetic Bragg peaks overlap with intense nuclear peaks, where the magnetic contribution is small. The purely magnetic Bragg peaks in the low-Q region are shown in Figs. 3(c)-(f). Not all of these peaks are reproduced perfectly because the parameters are adjusted to fit the global diffraction pattern and reduce the R-factor, as shown in Fig. 3(a). In particular, the (300) intensity is highly underestimated. This is probably because the magnetic form factor used for the analysis was for localized Mn moments with isotropic orbital distribution. Therefore, more accurate magnetic form factor, which includes the itineracy and/or anisotropic orbital nature of the Mn moments, should be used in order to have better agreement between the observed and calculated intensities.

The moment along the a and c axis were fitted to be $0.83(7)\mu_B$ and $0.88(5)\mu_B$, respectively, with the total moment of $1.2(1)\mu_B$. The magnetic R factor is 13.3% with the nuclear Bragg R factor of 5.30%. The magnetic moments at the four Mn sites are listed in Table III. The noncollinear magnetic structure determined by the analysis is shown in Fig. 1. The Mn1 and Mn4 moments and the Mn2 and Mn3 moments are antiparallel, whereas the Mn1 and Mn2 moments and the Mn3 and Mn4 moments are almost orthogonal.

IV. DISCUSSION

We found that the magnetic structure is noncollinear, in which the a and c axis magnetic components align antiferromagnetically and ferromagnetically along the zigzag chain, respectively. The magnetic structure is described by a combination of the two irreducible representations, suggesting that the symmetry of the magnetic structure is lower than the one expected from $Pnma$. Here, we will discuss how the magnetic structure can be realized. Although the electrical conductivity is metallic and the magnetic moment is reduced, the magnetic structure was found to be the one with $\boldsymbol{Q}_{\mathbf{m}}$=(0, 0, 0), suggesting that spin density wave is not the ground state so that the localized moment model may work to understand the magnetic interactions between Mn moments. The magnetic exchange interactions of the nearest-neighbor (J_1), second-neighbor (J_2), third-neighbor (J_3), and fourth-neighbor (J_4) were assumed to describe the magnetic

TABLE II. Possible magnetic structures for *Pnma* space group with $\boldsymbol{Q}_{\mathbf{m}}$=(0, 0, 0). u, v, and w represent the magnetic moment components along the a, b, and c axes, respectively.

Irreducible Representation	Mn1	Mn2	Mn3	Mn4
	(x, y, z)	$(-x+1/2, -y, z+1/2)$	$(-x, y+1/2, -z)$	$(x+1/2, -y+1/2, -z+1/2)$
Γ_1	$(0, v, 0)$	$(0, -v, 0)$	$(0, v, 0)$	$(0, -v, 0)$
Γ_2	$(u, 0, w)$	$(-u, 0, w)$	$(-u, 0, -w)$	$(u, 0, -w)$
Γ_3	$(u, 0, w)$	$(-u, 0, w)$	$(u, 0, w)$	$(-u, 0, w)$
Γ_4	$(0, v, 0)$	$(0, -v, 0)$	$(0, -v, 0)$	$(0, v, 0)$
Γ_5	$(0, v, 0)$	$(0, v, 0)$	$(0, v, 0)$	$(0, v, 0)$
Γ_6	$(u, 0, w)$	$(u, 0, -w)$	$(-u, 0, -w)$	$(-u, 0, w)$
Γ_7	$(u, 0, w)$	$(u, 0, -w)$	$(u, 0, w)$	$(u, 0, -w)$
Γ_8	$(0, v, 0)$	$(0, v, 0)$	$(0, -v, 0)$	$(0, -v, 0)$

TABLE III. Magnetic moments at the four Mn sites at T=9 K. The unit of the magnetic moments is μ_{B}.

site	u	v	w
Mn1	0.83(7)	0	0.88(5)
Mn2	0.83(7)	0	−0.88(5)
Mn3	−0.83(7)	0	0.88(5)
Mn4	−0.83(7)	0	−0.88(5)

structure. These interactions are indicated in Fig. 1 and the detailed geometrical parameters of the interactions are shown in Table IV. J_1 and J_2 are intrachain and J_3 and J_4 are interchain couplings. For J_1, where the distance is 2.64 Å, the direct exchange can be dominant. The superexchange interactions via Mn-P-Mn paths are expected to be dominant for other interactions.

Before conducting the neutron powder diffraction measurement, we initially predicted that the magnetic structure would be incommensurate due to competing J_1 and J_2. However, since J_2 is a superexchange coupling with a bonding angle of 100.24 deg and considered to be ferromagnetic, there should be no competition between J_1 and J_2 irrespective of the sign of J_1 and therefore an interaction model with J_1 and J_2 does not reproduce the non-colinear magnetic structure in Fig. 1. Then, J_3 and J_4 should be included in addition to J_1. As shown in Fig. 1, J_1, J_3, and J_4 form a triangle. The direction of moments connected with J_3 are antiparallel, whereas the direction of moments connected with J_1 and J_4 are almost orthogonal. If one or three bonds out of the three magnetic bonds are antiferromagnetic, the three interactions competes. This suggests that J_3 is a dominant interaction which is antiferromagnetic and both J_1 and J_4 are either ferromagnetic or antiferromagnetic. Since J_3 and J_4 are superexchange Mn-P-Mn couplings with bonding angles of 121.76 and 129.81 deg, respectively, both interactions are considered to be antiferromagnetic, indicating that J_1 is also antiferromagnetic. As described in Sec. IIIA, the structural study suggests an anomalous temperature dependence of the lattice constants, indicating a magnetoelastic coupling. The Mn-P-Mn bond angles for J_3 and J_4 are found to be slightly increased at 200 K, which is consistent with the stabilization of the antiferromagnetic couplings due to the magnetoelastic coupling.

Are the four magnetic interactions (J_1, J_2, J_3, and J_4) discussed above consistent with the $\boldsymbol{Q}_{\mathbf{m}}$=(0, 0, 0) magnetic structure? As shown in Fig. 1(c), there are two antiferromagnetic sublattices, constructed by the dominant J_3. One is a sublattice with Mn1 and Mn4 and the other is with Mn2 and Mn3. The two sublattices are connected with J_1 and J_4. The dominant antiferromagnetic J_3 keeps the magnetic structure commensurate with the primitive unit cell along the a axis. The inter-sublattice couplings, J_1 and J_4, keep the relative angles between the neighboring inter-sublattice spins same, *i.e.* $\alpha_{1-3'}$=$\alpha_{2-4'}$ and α_{1-2}=α_{3-4}=$\alpha_{1-2'}$=$\alpha_{3-4'}$, where α_{i-j} represents relative angle between Mni and Mnj moments. Because of these relations, the directions of the Mn2 and Mn2′ moments as well as those of the Mn4 and Mn4′ moments should be the same, which makes the magnetic structure commensurate along the b and c axes. Even if the ratios between J_1, J_3, and J_4 change, only the relative angle between the neighboring inter-sublattice moments changes without changing the magnetic unit cell. It is possible that the magnetic correlations become incommensurate along the b axis when J_2 is antiferromagnetic and compete with J_1. However, as mentioned above, J_2 is considered to be ferromagnetic. Therefore, the $\boldsymbol{Q}_{\mathbf{m}}$=(0, 0, 0) magnetic structure is consistent with the model with the four magnetic interactions.

The localized picture model suggests that the magnetic structure with $\boldsymbol{Q}_{\mathbf{m}}$=(0, 0, 0) is formed by the frustration among several exchange couplings. Since there is no inversion symmetry at the center of the second, third, and fourth-neighbor Mn bonds in NbMnP, the DM interaction may remain finite between them. The DM interaction for the third-neighbor Mn bond as well as the frustrated interactions could induce the non-collinear magnetic structure in the ac plane. Further studies are required to understand the magnetic interactions in more detail. In particular, an inelastic neutron scattering study using single crystals is desirable to determine the magnetic interactions accurately.

Here, the magnetic interactions considered above will be compared to those in the materials previously reported. The magnetic structures of the TiNiSi-type structure compounds RMnSi with R=Ho, Lu, and $Sc_{0.9}Lu_{0.1}$ were previously reported [19]. In HoMnSi,

TABLE IV. Bonding distances and angles of the Mn-P-Mn bonds at T=293 and 200 K obtained using the structural parameters shown in Table I.

$T = 293$ K			
Interaction	Mn-Mn distance (Å)	Mn-P distance (Å)	Mn-P-Mn angle (°)
J_1	2.6367(8)	2.3113(7), 2.365(1)	68.64(3)
J_2	3.5568(3)	2.3113(7)	100.61(5)
J_3	4.1396(8)	2.3647(11), 2.3749(11)	121.71(5)
J_4	4.2409(4)	2.3113(7), 2.3749(11)	129.63(3)

$T = 220$ K			
Interaction	Mn-Mn distance (Å)	Mn-P distances (Å)	Mn-P-Mn angle (°)
J_1	2.6370(8)	2.3132(8), 2.3669(11)	68.58(3)
J_2	3.5504(3)	2.3132(8)	100.24(5)
J_3	4.1415(8)	2.3669(11), 2.3738(11)	121.76(5)
J_4	4.2448(4)	2.3132(8), 2.3738(11)	129.81(3)

both Ho and Mn moments order. The Mn moments show collinear antiferromagnetic order at high temperatures. At low temperatures, a spiral component appears additionally, which give rises to a conical structure. In LuMnSi and $Sc_{0.9}Lu_{0.1}MnSi$, only Mn carries magnetic moment. The magnetic propagation vectors are incommensurate with (δ, 0, 0) and the magnetic structures are spiral. Therefore, the magnetic structures in RMnSi are different from that in NbMnP, although the ac easy plane in $Sc_{0.9}Lu_{0.1}MnSi$ is the same as in NbMnP. Interestingly, the magnetic interactions in RMnSi were reported to be the R size dependent. The magnetic structure in HoMnSi suggests that J_1 and J_4 are antiferromagnetic and J_3 is ferromagnetic or weakly antiferromagnetic. With decreasing the R size, J_1 seems to be less dominant and J_3 becomes more dominant and antiferromagnetic. The spiral structure with $\boldsymbol{Q}_{\mathbf{m}}$=($\delta$, 0, 0) should need competing interactions along the a axis. Since J_1, J_3, and J_4 are relevant to the coupling along the a axis, appropriate ratios between antiferromagnetic J_1, J_3, and J_4 are essential to realize the spiral structure.

It was also reported in Ref. [19] that, with decreasing the R size, the ordered magnetic moment decreases from 2.67μ_B with the nearest-neighbor Mn-Mn distance d_{Mn-Mn}∼2.94 Å in HoMnSi to 1.53μ_B with d_{Mn-Mn}∼2.74 Å in $Sc_{0.9}Lu_{0.1}MnSi$. This trend is consistent with the ordered moment of 1.2(1)μ_B with d_{Mn-Mn}=2.6370(8) Å in NbMnP, suggesting that the itineracy of the Mn moments is larger in NbMnP.

A characteristic feature in NbMnP is that a weak ferromagnetic component appears below T_N. Since the ferromagnetic component appears exactly below T_N and the magnetic susceptibility measurement was performed using single crystals, it is very likely that the ferromagnetic component is intrinsic and does not originate from impurities. There are at least two magnetic structure models, which are combinations of the irreducible representations allowed from the $Pnma$ structural symmetry, to explain the weak ferromagnetic component. The first model is most straightforward. The ferromagnetic component along the b axis with Γ_5 can simply be added to the $\Gamma_6 + \Gamma_7$ structure and the magnetic moments at the four Mn sites are Mn1: $(u, \Delta v, w)$, Mn2: $(u, \Delta v, -w)$, Mn3: $(-u, \Delta v, w)$, and Mn4: $(-u, \Delta v, -w)$. The second model is that there exist finite u in Γ_7 and the magnetic moments at the four Mn sites are Mn1: $(u + \Delta u, 0, w)$, Mn2: $(u + \Delta u, 0, -w)$, Mn3: $(-u + \Delta u, 0, w)$, and Mn4: $(-u + \Delta u, 0, -w)$. This component gives rise to a ferromagnetic component along the a axis. In addition this increases the magnetic moments at Mn1 and Mn2 and reduce those at Mn3 and Mn4. This magnetic structure also involves a slight rotation of magnetic moments in the ac plane from the magnetic structure described in Sec. IIIB. It is noted that the component was assumed to be zero in the magnetic structure analysis in order to reduce the number of fitting parameters, as described in Sec. IIIB. The ferromagnetic component along the a axis in the second model might be driven by the DM interactions for the third-neighbor Mn bond. It would be challenging to determine the most appropriate model for the ferromagnetic components using the neutron diffraction technique even using large crystals, because the ferromagnetic component is a factor of 1,000 smaller than the Mn moment.

In a Weyl semimetal Mn_3Sn, which consists of distorted kagome lattice of Mn moments and shows an inverse triangular spin structure with the negative sign of the vector chirality [20–22], a weak ferromagnetism with several milli-μ_B/f.u. in the kagome plane was observed [23]. The inverse triangular spin structure is stabilized by a DM and frustrated interactions. Furthermore, the ferromagnetic component, which is consistent with the structural symmetry with the magnetic propagation vector $\boldsymbol{Q}_{\mathbf{m}}$=(0, 0, 0), is considered to be due to the DM interaction. The domain of the ferromagnetic component, which originates from a rotation of Mn moments driven by a weak inplane magnetic anisotropy, can be flipped with weak magnetic field. This mechanism is ascribed to anomalous Hall and Nernst effects observed in this material [23, 24]. The ferromagnetic component of

milli-μ_B/f.u. plays an important role in exhibiting the anomalous phenomena. It would be interesting to investigate if NbMnP also exhibits the similar properties when large crystals become available in the future.

V. SUMMARY

The bulk properties and magnetic structure in NbMnP were studied. The magnetic susceptibility as well as the resistivity shows an anomaly at 233 K, which indicates an antiferromagnetic phase transition. A weak ferromagnetic component of $\sim 0.0015\mu_B$/f.u. was also observed below T_N. Neutron powder diffraction measurements reveals that the magnetic structure is a noncollinear structure, in which the magnetic symmetry is lower than the one expected from *Pnma* and the arrangements of the magnetic components along the a and c axis are antiferromagnetic and ferromagnetic along the zigzag chain direction, respectively. NbMnP has largely itinerant Mn moments ($1.2\mu_B$) among the materials with the TiNiSi-type structure. Using the localized moment model, we discussed the possible magnetic interactions in this material. It is likely that the antiferromagnetic intrachain (J_1) and interchain (J_3 and J_4) couplings are competing. The noncollinear magnetic structure can be realized by the competing interactions as well as the DM interaction. The weak ferromagnetic component might also be induced by the DM interaction. NbMnP is an antiferromagnetic metal, in which the bulk properties might be affected by the frustrated and DM interactions. We hope that our results stimulate further investigations in this interesting system.

ACKNOWLEDGMENTS

We thank Hideki Tou, Hisatomo Harima, Feng Ye, and S. Okamoto for valuable discussions. This work was supported by JSPS KAKENHI Grants [Nos. 15H05885, 15H05882, and 18H04321 (J-Physics)]. This research used resource at the Spallation Neutron Source, a DOE Office of Science User Facility operated by the Oak Ridge National Laboratory.

Appendix: Structural analysis using the neutron powder diffraction data

The results of the Rietveld refinement for the neutron powder diffraction data measured at 9 and 250 K are shown in Table V. The structural parameters are complementary to those determined using the X-ray diffraction data shown in Table I.

The Modified March's function for the preferred orientation factor along the b axis (F_{po}) was applied to analyze the 250 K data. In the function, $F_{po} < 1$, $F_{po} = 1$, and $F_{po} > 1$ correspond to platy habit, no preferred orientation, and needle-like habit, respectively. F_{po} was fitted to be 0.911(2). Although we expected to have slightly needle-like habit along the b axis, the analysis shows slightly platy habit. Since F_{pr} is close to 1, the powder sample is considered to be almost randomly oriented.

TABLE V. Structural parameters of NbMnP determined by the powder neutron structural analysis at T=250 K and 9 K.

$T = 250$ K						
Atom	position	x	y	z	$Occ.$	U(Å^2)
Nb	4c	0.0312(1)	0.2500	0.6720(1)	0.885(6)	0.073(17)
Mn	4c	0.1409(2)	0.2500	0.0593(2)	1	0.138(21)
P	4c	0.2676(1)	0.2500	0.3694(1)	1	0.106(17)

orthorhombic ($Pnma$): a=6.1664(1) Å, b=3.5463(1) Å, c=7.2042(1) Å, Bragg R factor=6.24%

$T = 9$ K						
Atom	position	x	y	z	$Occ.$	U(Å^2)
Nb	4c	0.0317(1)	0.2500	0.6715(1)	0.885	0.025(10)
Mn	4c	0.1411(2)	0.2500	0.0595(2)	1	0.004(17)
P	4c	0.2674(2)	0.2500	0.3688(1)	1	0.008(13)

orthorhombic ($Pnma$): a=6.1661(1) Å, b=3.5325(1) Å, c=7.2199(1) Å, Bragg R factor=5.30%

[1] I. Dzyaloshinskii, J. Phys. Chem. Solids **4**, 241 (1958).
[2] T. Moriya, Phys. Rev. **120**, 91 (1960).
[3] T. Yamazaki, Y. Tabata, T. Waki, T. J. Sato, M. Matsuura, K. Ohoyama, M. Yokoyama, and H. Nakamura, J. Phys. Soc. Jpn. **83**, 054711 (2014).
[4] N. Nagaosa and Y. Tokura, Nat. Nanotechnol., **8**, 899 (2013).
[5] S. Mühlbauer, B. Binz, F. Jonietz, C. Pfleiderer, A. Rosch, A. Neubauer, R. Georgii, P. Böni, Science **323**, 915 (2009).
[6] P. Bak and H. H. Jensen, J. Phys. C: Solid State Phys., **13**, L881 (1980).
[7] Y. F. Lomnitskaya, G. D. Kondratyuk, L. I. Zakharets, Zhurnal Neorganicheskoi Khimii **33**, 734 (1988).
[8] T. N. Lamichhane, V. Taufour, M. W. Masters, D. S. Parker, U. S. Kaluarachchi, S. Thimmaiah, S. L. Bud'ko, and P. C. Canfield, Appl. Phys. Lett. **109**, 092402 (2016).
[9] G.M. Sheldrick, Acta Crystallogr., Sect. A **64**, 112 (2008).
[10] A.L. Spek, J. Appl. Crystallogr. **36**, 7 (2003).
[11] A. Huq, J. P. Hodges, O. A. Gourdon, and L. Heroux, Zeitschrift fur Kristallographie, **1**, 127 (2011).
[12] J. Rodriguez-Carvajal, Solid State Phenom. **170**, 263 (2011).
[13] J. Rodriguez-Carvajal, Physica B **192**, 55 (1993).
[14] Y. Kuwata, H. Kotegawa, H. Tou, H. Harima, Q.-P. Ding, K. Takeda, J. Hayashi, E. Matsuoka, H. Sugawara, T. Sakurai, H. Ohta, and Y. Furukawa, Phys. Rev. B **102**, 205110 (2020).
[15] S. Tomiyoshi, H. Yoshida, H. Ohmori, T. Kaneko, and H. Yamatomo, J. Mag. Mag. Mater. **70**, 247 (1987).
[16] J.-G. Cheng, K. Matsubayashi, W. Wu, J. P. Sun, F. K. Lin, J. L. Luo, and Y. Uwatoko, Phys. Rev. Lett. **114**, 117001 (2015).
[17] H. Kotegawa, M. Matsuda, F. Ye, Y. Tani, K. Uda, Y. Kuwata, H. Tou, E. Matsuoka, H. Sugawara, T. Sakurai, H. Ohta, H. Harima, K. Takeda, J. Hayashi, S. Araki, and T. C. Kobayashi, Phys. Rev. Lett. **124**, 087202 (2020).
[18] F. P. Mena, D. van der Marel, A. Damascelli, M. Fäth, A. A. Menovsky, J. A. Mydosh, Phys. Rev. B **67**, 241101(R) (2003).
[19] G. Venturini, I. Ijjaali, E. Ressouche, and B. Malaman, J. Alloys Compounds **256**, 65 (1997).
[20] S. Tomiyoshi and Y. Yamaguchi, J. Phys. Soc. Jpn. **51**, 2478 (1982).
[21] P. J. Brown, V. Nunez, F. Tasset, J. B. Forsyth, and P. Radhakrishna, J. Phys. Condens. Matter **2**, 9409 (1990).
[22] T. Nagamiya, S. Tomiyoshi, and Y. Yamaguchi, Solid State Commun. **42**, 385 (1982).
[23] S. Nakatsuji, N. Kiyohara, and T. Higo, Nature **527**, 212 (2015).
[24] M. Ikhlas, T. Tomita, T. Koretsune, M.-T. Suzuki, D. Nishio-Hamane, R. Arita, Y. Otani, and S. Nakatsuji. Nat. Phys. **13**, 1085 (2017).